IJCRT.ORG ISSN : 2320-2882

INTERNATIONAL JOURNAL OF CREATIVE RESEARCH THOUGHTS (IJCRT)

An International Open Access, Peer-reviewed, Refereed Journal

Transient Finite Element Analysis Of Aluminium Stiffened Sandwich Plates: Comparative Study Of Rectangular, Hexagonal, And Triangular Stiffener Configurations

[1]Mr. Naik Aniket Gopalrao, [2]Prof. J M Chavan

[1]M.Tech Student, [2]Assistant Professor

[12] Department of Civil Engineering

M.B.E.S. College of Engineering, Ambajogai, Maharashtra, India

Abstract: Aluminium stiffened sandwich plates are extensively used in marine, aerospace, and civil engineering due to their excellent stiffness-to-weight ratio. Under dynamic service conditions these structures are subjected to transient loads whose effects cannot be captured by static analysis alone. This study presents a systematic three-dimensional transient finite element analysis (FEA) of Al 6061-T6 aluminium stiffened sandwich plates using ANSYS Workbench 18.2. Three stiffener geometries — rectangular, hexagonal, and triangular — are comparatively evaluated under sinusoidal and Hanning-windowed nodal forces of 1000 N amplitude at excitation frequencies of 100 kHz, 150 kHz, and 200 kHz. The base plate dimensions are 1200 mm × 1200 mm × 3 mm with all four edges fully clamped; stiffener height is 50 mm and thickness is 5 mm. Directional deformation is extracted at nine pre-defined nodes. Results establish that the triangular stiffener configuration achieves the lowest peak central-node deformation — 0.350 µm at 100 kHz, which is 42.3% lower than the rectangular configuration (0.608 µm) and 60.4% lower than the hexagonal configuration (0.883 µm). Peak deformation decreases monotonically with increasing excitation frequency for all configurations. At 200 kHz, triangular and hexagonal configurations converge to 0.150 µm, indicating dominance of local inertial effects. Hanning-windowed loading produces deformations approximately six orders of magnitude lower than sinusoidal loading. The triangular stiffener is identified as the optimal configuration for dynamic centralised loading applications.

Index Terms — Aluminium sandwich plate, ANSYS Workbench, directional deformation, Hanning window, stiffener geometry, transient FEA.

I. INTRODUCTION

Stiffened sandwich plates are widely deployed in marine, aerospace, civil, and offshore structural applications owing to their superior stiffness-to-weight ratio. By combining thin face sheets with an internal rib network, these assemblies achieve elevated bending resistance and buckling strength per unit mass relative to monolithic plate sections [1]. In service, such structures are routinely subjected to time-varying dynamic loading — arising from impact events, wave slamming, blast pressure waves, seismic ground motion, and moving vehicles — that may produce significant dynamic amplification not captured by conventional static analysis [2].

Aluminium alloy 6061-T6, characterised by density 2700 kg/m³, Young's modulus 70 GPa, and yield strength 276 MPa, is the predominant material for stiffened sandwich plates in high-speed marine and aerospace applications [3]. Its relatively low elastic modulus compared with steel increases susceptibility to dynamic deformation, making accurate transient FEM analysis essential. Among the stiffener geometries employed in practice, rectangular arrangements are most conventional; hexagonal and triangular arrangements potentially offer superior load distribution, yet systematic comparisons under transient loading have not been reported.

This study addresses this gap through a systematic ANSYS-based transient FEM analysis of Al 6061-T6 stiffened sandwich plates with rectangular, hexagonal, and triangular stiffener configurations. Sinusoidal and Hanning-windowed loading are applied at 100 kHz, 150 kHz, and 200 kHz. Directional deformation is extracted at nine nodes per case, enabling quantitative comparison of peak dynamic response and spatial attenuation characteristics across all configurations.

II. Literature Review

Aradhye and Joglekar [4] performed three-dimensional transient FEM analyses of honeycomb composite sandwich structures, demonstrating that guided-wave wavefields are sensitive to core-thickness variation, enabling structural health monitoring. Capineri and Bulletti [5] reviewed UGW sensing technology for SHM, establishing that piezoelectric-based systems can locate impacts with centimetre-scale accuracy on plate-like structures.

Shen et al. [6] proposed a convolutional neural network approach trained on wavelet-transformed FEM-generated guided-wave responses, achieving approximately 99% damage detection accuracy for stiffened plates. Hosseinabadi and Khedmati [7] reviewed ultimate strength behaviour of aluminium structural elements, identifying heat-affected zone strength reduction and the rounded stress-strain knee as primary challenges in aluminium design, and validated modified empirical models against extensive FEM databases.

Kim et al. [8] derived an empirical formula for the ultimate compressive strength of stiffened panels by generating a large ANSYS parametric database varying plate slenderness, column slenderness, and stiffener section. Singh and Duggal [9] demonstrated via three-dimensional FEM that increasing stiffener cross-section aspect ratio reduces maximum plate deflection under lateral pressure by up to 68% relative to the unstiffened plate. Goel et al. [10] showed that aluminium foam-core sandwich panels reduce peak blast impulse by up to 55% compared with equivalent solid steel plates. Anyfantis [11] found that non-uniform in-plane thrust can reduce the ultimate compressive strength of ship hull stiffened panels by up to 35%. De Queiroz et al. [12] applied constructal design theory to optimise stiffened corrugated panels, establishing that diminishing returns in deflection reduction occur beyond a stiffener height-to-thickness ratio of 20.

The foregoing review identifies five research gaps motivating the present study: (i) scarcity of transient FEM studies specifically on aluminium stiffened sandwich plates; (ii) absence of comparative studies on rectangular, hexagonal, and triangular stiffener configurations under dynamic loading; (iii) limited frequency-dependent deformation analyses; (iv) lack of Hanning-windowed load studies alongside sinusoidal loading; and (v) limited material-specific transient studies for the Al 6061-T6 system.

III. Problem Formulation and Methodology

A. Structural Configuration

The base plate measures 1200 mm × 1200 mm × 3 mm. Three stiffener configurations are investigated, all with stiffener height 50 mm and thickness 5 mm: (i) Rectangular — orthogonal rib grid subdividing the plate into square cells; (ii) Hexagonal — honeycomb-pattern ribs; and (iii) Triangular — ribs arranged in a triangulated network forming equilateral-triangle cells. All components are fabricated from Al 6061-T6 whose properties are given in Table 1.

Table 1: Material Properties of Aluminium Alloy Al 6061-T6

Property	Value
Young's Modulus (E)	70 GPa
Poisson's Ratio (ν)	0.33
Density (ρ)	2700 kg/m³
Yield Strength (σy)	276 MPa
Ultimate Tensile Strength	310 MPa
Shear Modulus (G)	26.3 GPa

B. Finite Element Model

Three-dimensional CAD models were constructed in ANSYS DesignModeler. SOLID186 (20-node quadratic hexahedral) and SOLID187 (10-node quadratic tetrahedral) elements are employed, ensuring accurate three-dimensional stress state representation without shear locking. A global element size of 10 mm is applied with local refinement to 5 mm at stiffener-plate junctions. Mesh statistics are given in Table 2.

Table 2: Finite Element Mesh Details

Parameter	Rectangular	Hex / Triangular
Element type	SOLID186/187	SOLID186/187
Global element size	10 mm	10 mm
Approx. nodes	~185,000	~210,000
Approx. elements	~42,000	~48,000
Skewness (mesh quality)	< 0.4	< 0.4

C. Boundary Conditions and Loading

All four plate edges are fully clamped: translational (Ux = Uy = Uz = 0) and rotational (θx = θy = θz = 0) degrees of freedom are constrained, representative of welded connections in ship hull and offshore structures. The transient load (amplitude A = 1000 N) is applied at the plate centre as a concentrated nodal force using two waveforms:

Sinusoidal: $F(t) = A \cdot \sin(2\pi ft)$, applied for N = 4 cycles at f = 100, 150, and 200 kHz.

Hanning-windowed: $F(t) = A \cdot \sin(2\pi ft) \cdot [0.5 - 0.5 \cdot \cos(2\pi tf/N)]$, applied at f = 100 and 200 kHz for the rectangular configuration, producing a smooth-onset toneburst used in guided-wave NDE.

D. Solver Settings

The Newmark-beta implicit scheme (β = 0.25, γ = 0.5 — constant average acceleration, unconditionally stable) is used. The governing equations of motion are:

$$\mathbf{[M]\{\ddot{u}\} + [C]\{\dot{p}\} + [K]\{u\} = \{F(t)\}}$$

Damping [C] = 0, providing conservative upper-bound deformation estimates. Automatic time-stepping is applied with initial time step 1/20 of the excitation period. Directional (z-axis) deformation is extracted at nine nodes: Node 1 at the plate centre and Nodes 2–9 distributed radially outward exploiting bi-axial symmetry.

IV. RESULTS AND DISCUSSION

A. Rectangular Stiffener — Sinusoidal Loading

Figures 1–3 show the ANSYS model geometry, mesh, and fixed boundary conditions for the rectangular stiffener configuration.

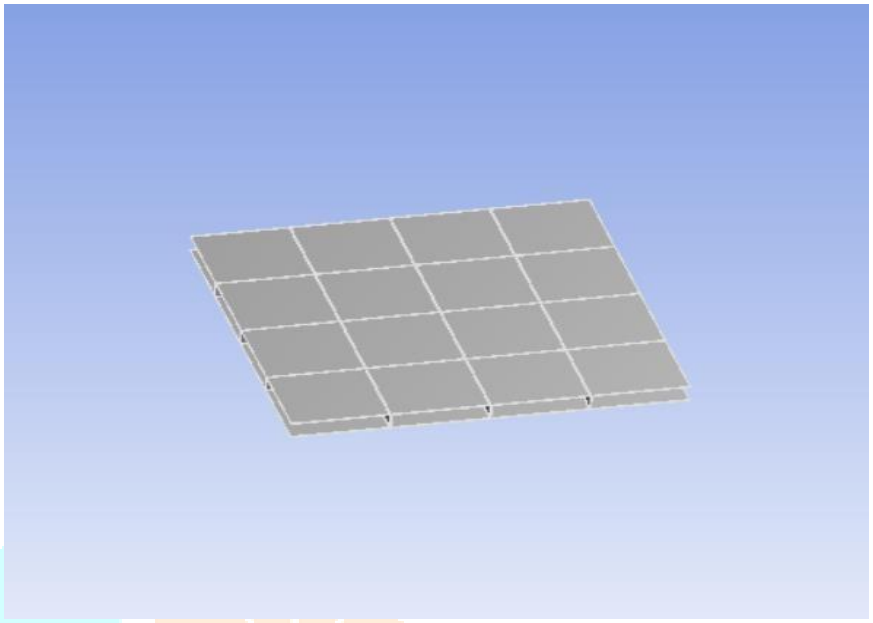

Fig. 1. Geometry of rectangular stiffened sandwich plate

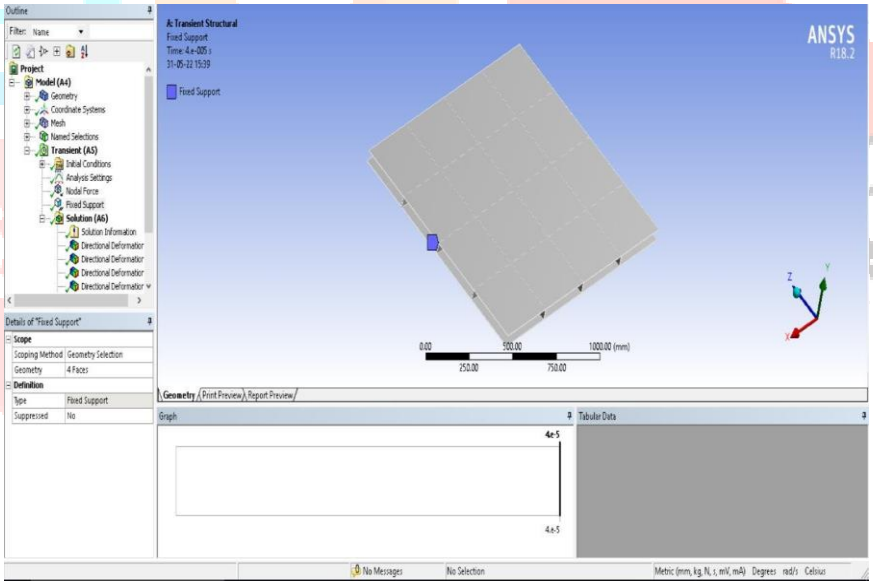

Fig. 2. Fixed boundary conditions — rectangular configuration

Table 3 presents directional deformation at 100 kHz. The peak positive deformation at Node 1 (plate centre, loaded point) is 6.0771×10^{-4} m (0.608 μm). Deformation attenuates rapidly with radial distance from the loading point; Node 4, nearest to the clamped edge, records only 3.0499×10^{-5} m — a 95% reduction. Symmetry of values at paired nodes (6 & 8; 7 & 9) confirms correct boundary condition application.

Table 3: Directional Deformation — Rectangular Stiffener, Sinusoidal 100 kHz

No.	Node	Directional Deformation (m)	
		Maximum	Minimum
1	Node 1	6.0771e-4	-3.4871e-4
2	Node 2	6.2289e-5	-7.2090e-5
3	Node 3	4.5310e-5	-5.0762e-5
4	Node 4	3.0499e-5	-3.5718e-5
5	Node 5	7.5955e-5	-5.9597e-5
6	Node 6	3.9882e-5	-4.9260e-5
7	Node 7	4.6149e-5	-3.9814e-5
8	Node 8	3.9882e-5	-4.9260e-5
9	Node 9	4.6149e-5	-3.9814e-5

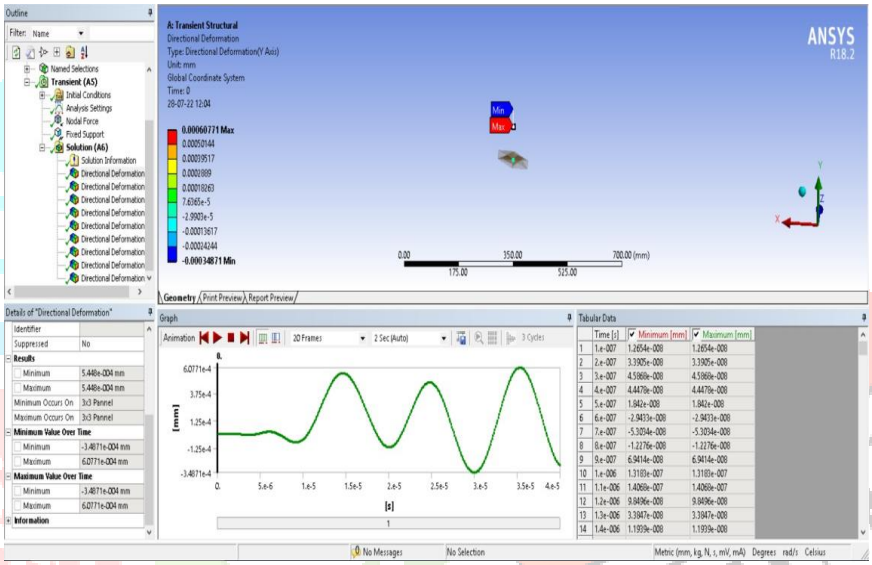

Fig. 3. Directional deformation contour — rectangular stiffener, sinusoidal 100 kHz

Table 4: Directional Deformation — Rectangular Stiffener, Sinusoidal 150 kHz

No.	Node	Directional Deformation (m)	
		Maximum	Minimum
1	Node 1	3.6558e-4	-1.0253e-4
2	Node 2	2.5975e-5	-1.9997e-5
3	Node 3	1.2766e-5	-1.6905e-5
4	Node 4	1.5631e-5	-2.1937e-5
5	Node 5	1.9026e-5	-2.5989e-5
6	Node 6	2.4575e-5	-2.4345e-5
7	Node 7	3.3570e-5	-2.8108e-5
8	Node 8	2.4575e-5	-2.4345e-5
9	Node 9	3.3570e-5	-2.8108e-5

At 150 kHz (Table 4), peak deformation decreases to 3.6558 × 10^{-4} m, a 39.8% reduction from 100 kHz, attributable to the shorter loading period leaving less time for displacement accumulation before each load reversal.

Table 5: Directional Deformation — Rectangular Stiffener, Sinusoidal 200 kHz

No.	Node	Directional Deformation (m)	
		Maximum	Minimum
1	Node 1	2.4111e-4	-1.0838e-4
2	Node 2	1.2150e-5	-1.6258e-5
3	Node 3	1.3924e-5	-9.7883e-6
4	Node 4	1.5107e-5	-4.2940e-6
5	Node 5	2.8278e-5	-1.2244e-5
6	Node 6	8.7848e-6	-1.0787e-5
7	Node 7	1.7256e-5	-1.7828e-5
8	Node 8	8.7848e-6	-1.0787e-5
9	Node 9	1.7256e-5	-1.7828e-5

At 200 kHz (Table 5), peak deformation further decreases to 2.4111 × 10^{-4} m, a 34.1% reduction from 150 kHz. The monotonic frequency-dependent reduction is consistent across all three configurations.

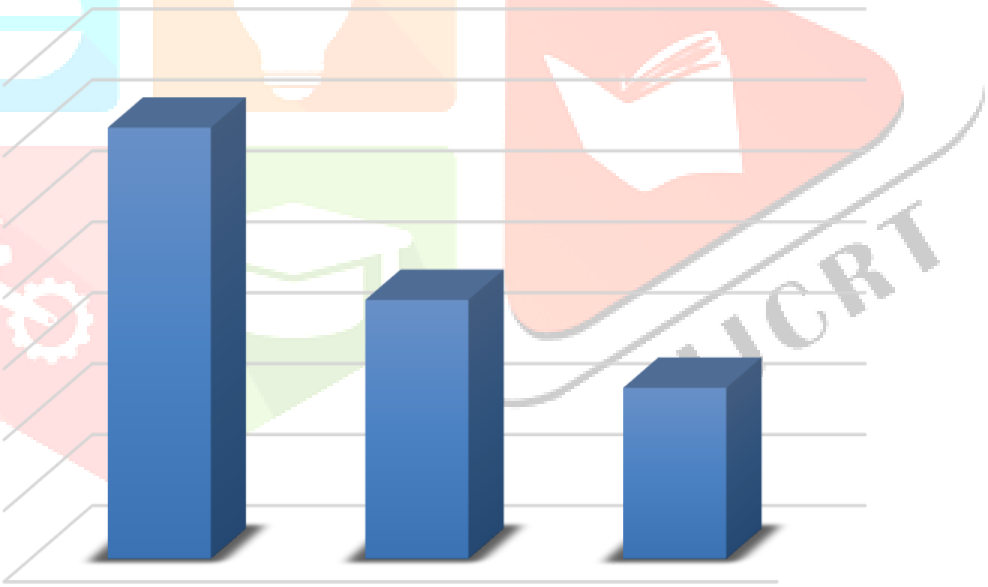

Fig. 4. Peak central-node deformation vs. excitation frequency — rectangular stiffener

B. Hexagonal Stiffener — Sinusoidal Loading

Table 6 presents results for the hexagonal configuration at 100 kHz. The peak deformation is 8.8313 × 10^{-4} m (0.883 µm), exceeding the rectangular result by 45.4%. This higher compliance arises from two geometric factors: (i) fewer load-carrying ribs per unit plate area pass through the central zone in the hexagonal cell pattern, and (ii) the 120° internal angles of hexagonal cells provide lower in-plane shear resistance than the orthogonal rectangular grid.

Table 6: Directional Deformation — Hexagonal Stiffener, Sinusoidal 100 kHz

No.	Node	Directional Deformation (m)	
		Maximum	Minimum
1	Node 1	8.8313e-4	-3.6555e-4
2	Node 2	2.8299e-5	-3.2472e-5
3	Node 3	3.6238e-5	-4.0494e-5
4	Node 4	1.9807e-5	-2.0466e-5
5	Node 5	3.6013e-5	-4.0197e-5
6	Node 6	2.4171e-5	-2.1605e-5
7	Node 7	6.7401e-6	-1.7886e-5
8	Node 8	7.6946e-6	-9.2976e-6
9	Node 9	8.7114e-6	-1.2683e-5

Table 7: Directional Deformation — Hexagonal Stiffener, Sinusoidal 150 kHz

No.	Node	Directional Deformation (m)	
		Maximum	Minimum
1	Node 1	5.9151e-4	-3.7373e-4
2	Node 2	5.5977e-5	-4.9753e-5
3	Node 3	1.0527e-5	-7.7682e-6
4	Node 4	8.5396e-6	-5.4718e-6
5	Node 5	1.8934e-5	-1.9693e-5
6	Node 6	1.4944e-5	-1.4211e-5
7	Node 7	3.8252e-6	-6.6371e-6
8	Node 8	7.7082e-6	-7.4232e-6
9	Node 9	4.5564e-6	-1.6214e-6

Table 8: Directional Deformation — Hexagonal Stiffener, Sinusoidal 200 kHz

No.	Node	Directional Deformation (m)	
		Maximum	Minimum
1	Node 1	1.5015e-4	-1.0599e-4
2	Node 2	9.5094e-7	-5.1318e-7
3	Node 3	1.9113e-6	-7.4026e-7
4	Node 4	1.6738e-6	-1.1055e-6
5	Node 5	1.3607e-6	-1.8274e-6
6	Node 6	3.1212e-7	-2.1461e-7
7	Node 7	9.6853e-7	-1.9169e-6
8	Node 8	3.8747e-7	-2.9735e-7
9	Node 9	8.3605e-7	-1.5432e-6

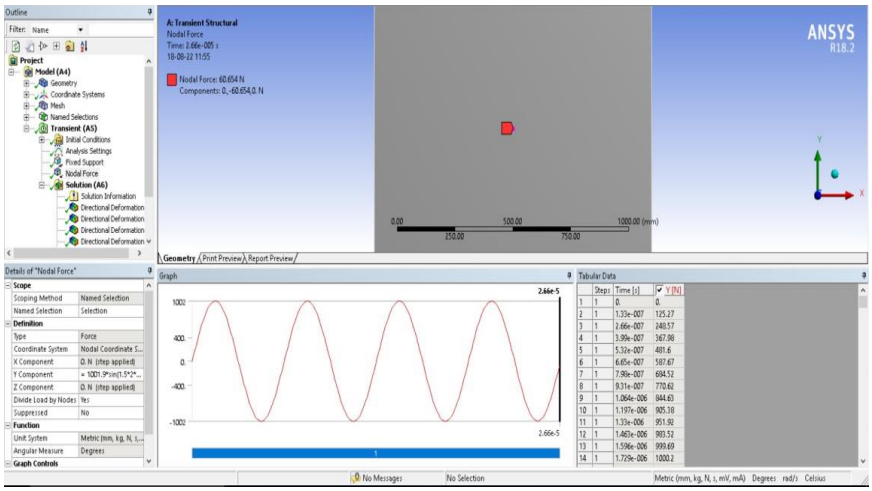

Fig. 5. Directional deformation contour — hexagonal stiffener, sinusoidal 100 kHz

C. Triangular Stiffener — Sinusoidal Loading

Table 9 presents results for the triangular configuration at 100 kHz. The peak central-node deformation is 3.5009×10^{-4} m (0.350 µm) — 42.3% lower than the rectangular configuration and 60.4% lower than the hexagonal configuration. The triangulated rib network transfers applied forces predominantly through axial rib action (tension/compression) rather than bending, analogous to a statically determinate truss, providing the highest effective dynamic stiffness of the three configurations studied.

Table 9: Directional Deformation — Triangular Stiffener, Sinusoidal 100 kHz

No.	Node	Directional Deformation (m)	
		Maximum	Minimum
1	Node 1	3.5009e-4	-3.0563e-4
2	Node 2	4.0635e-6	-4.6643e-6
3	Node 3	7.3532e-6	-8.8780e-6
4	Node 4	9.0477e-6	-9.8517e-6
5	Node 5	1.3871e-5	-1.5951e-5
6	Node 6	-1.9047e-6	-1.9047e-6
7	Node 7	6.6951e-6	-8.5207e-6
8	Node 8	2.7194e-6	6.6951e-6
9	Node 9	-3.2162e-6	-3.2162e-6

Table 10: Directional Deformation — Triangular Stiffener, Sinusoidal 150 kHz

No.	Node	Directional Deformation (m)	
		Maximum	Minimum
1	Node 1	1.9887e-4	-9.8769e-5
2	Node 2	1.6209e-6	-3.5882e-6
3	Node 3	1.3712e-6	-4.2885e-6
4	Node 4	1.9147e-6	-1.8924e-6
5	Node 5	4.0983e-6	-5.7434e-6
6	Node 6	5.5040e-7	-2.5656e-7
7	Node 7	4.4661e-6	-3.1644e-6
8	Node 8	7.7433e-7	-9.7146e-7
9	Node 9	2.5382e-6	-2.5423e-6

Table 11: Directional Deformation — Triangular Stiffener, Sinusoidal 200 kHz

No.	Node	Directional Deformation (m)	
		Maximum	Minimum
1	Node 1	1.5015e-4	-1.0599e-4
2	Node 2	9.5094e-7	-5.1318e-7
3	Node 3	1.9113e-6	-7.4026e-7
4	Node 4	1.6738e-6	-1.1055e-6
5	Node 5	1.3607e-6	-1.8274e-6
6	Node 6	3.1212e-7	-2.1461e-7
7	Node 7	9.6853e-7	-1.9169e-6
8	Node 8	3.8747e-7	-2.9735e-7
9	Node 9	8.3605e-7	-1.5432e-6

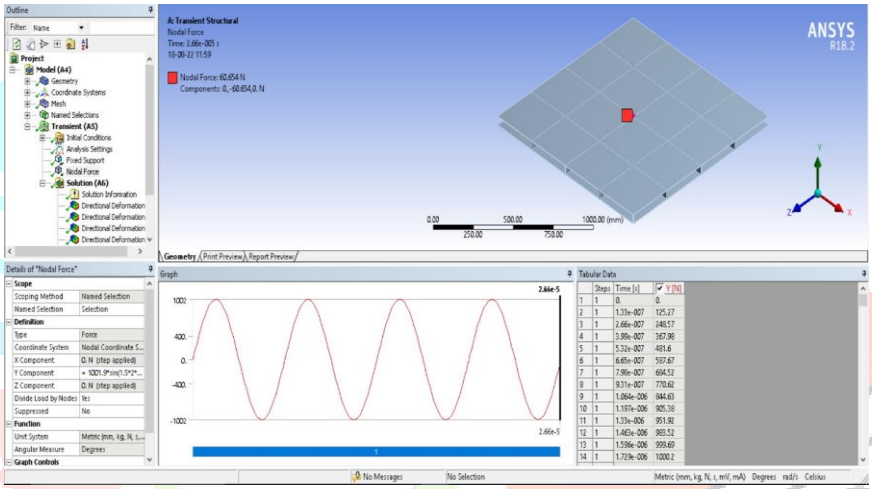

Fig. 6. Directional deformation contour — triangular stiffener, sinusoidal 100 kHz

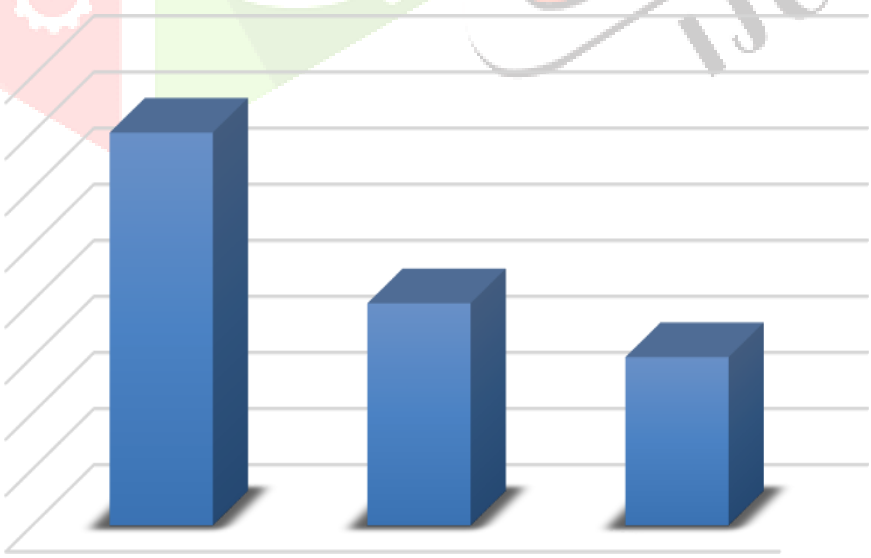

Fig. 7. Peak central-node deformation vs. excitation frequency — triangular stiffener

At 200 kHz, the triangular and hexagonal configurations converge to an identical peak deformation of 1.5015×10^{-4} m (0.150 µm). This convergence indicates that at sufficiently high frequencies, local inertial effects become dominant over stiffener-geometry-dependent bending stiffness differences, making the two configurations dynamically equivalent at this frequency.

D. Hanning-Windowed Loading

Tables 12 and 13 present deformation results under Hanning-windowed loading applied to the rectangular stiffener configuration at 100 kHz and 200 kHz, respectively.

Table 12: Directional Deformation — Rectangular, Hanning 100 kHz

No.	Node	Directional Deformation (m)	
		Maximum	Minimum
1	Node 1	-3.5595e-10	3.4432e-10
2	Node 2	-5.1309e-11	4.9947e-11
3	Node 3	-3.9653e-11	3.6715e-11
4	Node 4	-3.2593e-11	2.5722e-11
5	Node 5	-5.1243e-11	5.2932e-11
6	Node 6	-3.1140e-11	3.1366e-11
7	Node 7	-2.8470e-11	2.7637e-11
8	Node 8	-3.1140e-11	3.1366e-11
9	Node 9	-2.8470e-11	2.7637e-11

Table 13: Directional Deformation — Rectangular, Hanning 200 kHz

No.	Node	Directional Deformation (m)	
		Maximum	Minimum
1	Node 1	-1.1667e-10	1.0397e-10
2	Node 2	-7.5041e-12	9.0440e-12
3	Node 3	8.8169e-12	5.6999e-12
4	Node 4	-6.0467e-12	7.1376e-12
5	Node 5	-1.3205e-11	1.5562e-11
6	Node 6	-6.0493e-12	4.6930e-12
7	Node 7	-1.0525e-11	1.0307e-11
8	Node 8	-6.0493e-12	4.6930e-12
9	Node 9	-1.0525e-11	1.0307e-11

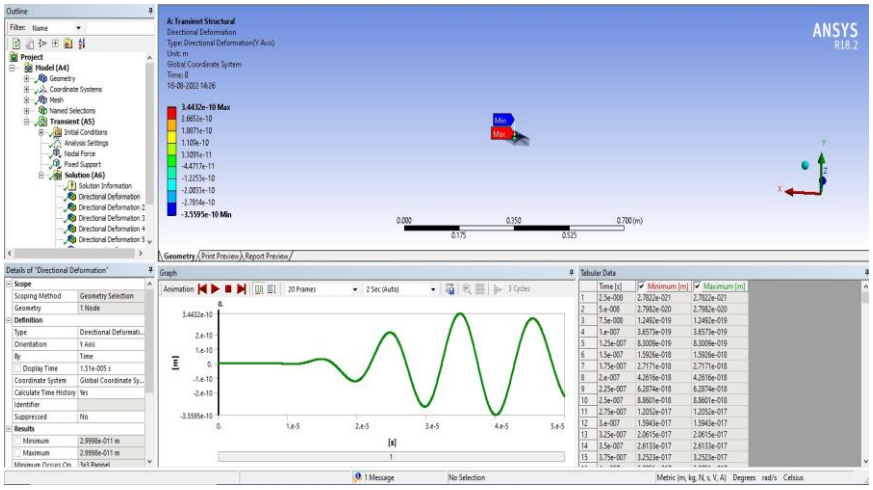

Fig. 8. Directional deformation — Hanning-windowed loading, 100 kHz, rectangular stiffener

The peak deformation under Hanning loading at 100 kHz is -3.5595×10^{-10} m, approximately six orders of magnitude smaller than the corresponding sinusoidal result. The Hanning-windowed toneburst concentrates its energy in a narrow frequency band and delivers only a single smooth pulse of net displacement, producing far smaller time-integrated structural excitation than the four-cycle sinusoidal input. At 200 kHz, the Hanning peak deformation (-1.1667×10^{-10} m) is 67.3% lower than at 100 kHz, confirming the frequency-dependent trend independently of waveform shape. These results confirm that Hanning-windowed excitation, as used in guided-wave NDE, does not produce structurally significant deformations.

E. Comparative Summary

Table 14 and Figures 9–10 summarise peak central-node deformation for all configurations and frequencies.

Table 14: Summary — Peak Central-Node Deformation (μm), Sinusoidal Loading

Stiffener Configuration	Peak Deformation (μm)		
	100 kHz	150 kHz	200 kHz
Rectangular	0.608	0.366	0.241
Hexagonal	0.883	0.592	0.150
Triangular (Optimal)	**0.350**	**0.199**	**0.150**

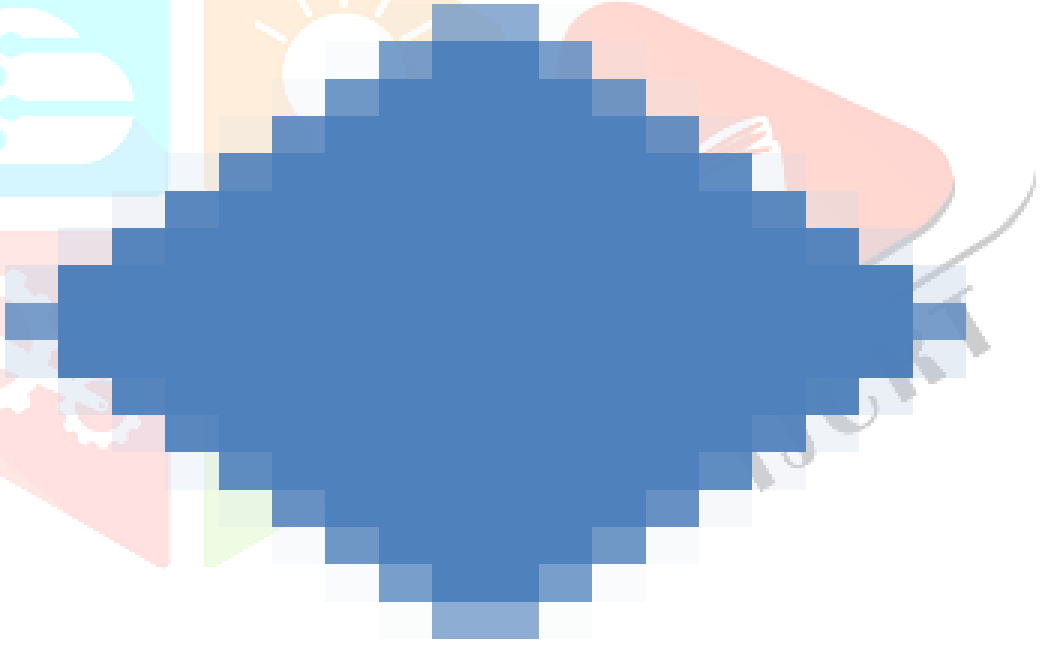

Fig. 9. Overall peak deformation comparison — all configurations and frequencies

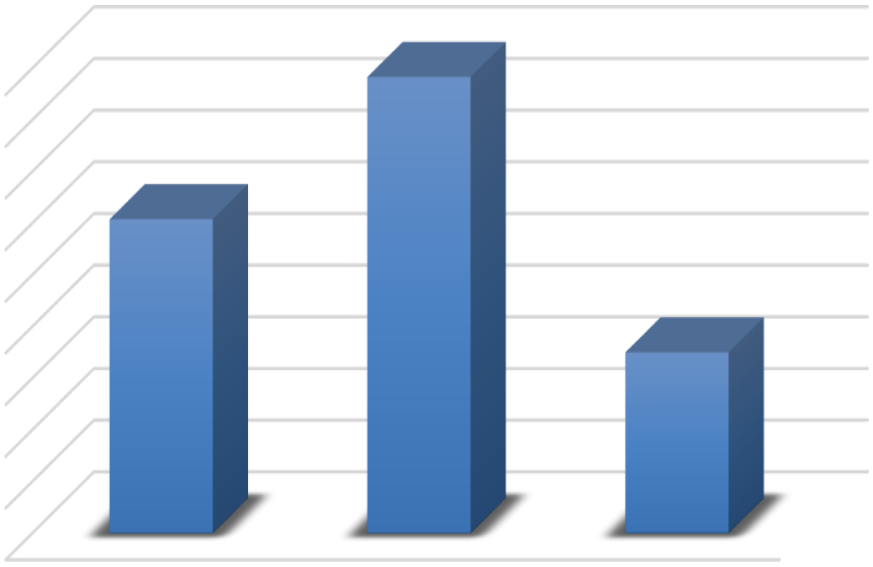

Fig. 10. Cross-configuration comparison at 100 kHz

Four key trends emerge from Table 14: (i) peak deformation decreases monotonically with increasing excitation frequency for all configurations; (ii) the triangular stiffener consistently achieves the lowest peak deformation at 100 kHz and 150 kHz; (iii) at 200 kHz, triangular and hexagonal configurations converge (0.150 µm each); and (iv) the hexagonal configuration exhibits the highest peak deformation at 100 kHz and 150 kHz, indicating it is the least structurally efficient geometry for centralised transient loading in this frequency range.

V. CONCLUSION

A systematic transient FEM analysis of Al 6061-T6 aluminium stiffened sandwich plates with rectangular, hexagonal, and triangular stiffener configurations has been performed using ANSYS Workbench 18.2. The following conclusions are drawn:

1. The triangular stiffener is the optimal geometry for centralised transient loading. At 100 kHz it achieves a peak deformation of 0.350 µm — 42.3% lower than rectangular (0.608 µm) and 60.4% lower than hexagonal (0.883 µm). The advantage arises from the triangulated force-path network that transfers load primarily through axial rib action, providing higher effective dynamic stiffness.
2. Peak deformation decreases monotonically with increasing excitation frequency for all configurations and both waveforms. For the rectangular configuration, reductions of 39.8% (100–150 kHz) and 34.1% (150–200 kHz) are observed.
3. Spatial deformation attenuation from the loaded centre to the clamped edges is 95–99% for all configurations, confirming that transient structural response is strongly localised near the excitation point.
4. At 200 kHz, triangular and hexagonal configurations converge to identical peak deformations (0.150 µm), indicating that local inertial effects dominate over stiffener-geometry-dependent stiffness differences beyond a threshold frequency.
5. Hanning-windowed loading produces deformations approximately six orders of magnitude lower than equivalent sinusoidal loading, confirming its structural safety for guided-wave NDE applications.

Future work should include experimental validation via laser Doppler vibrometry, extension to elasto-plastic material models (Johnson-Cook), topology optimisation under transient loading constraints, and investigation of hybrid stiffener arrangements.

REFERENCES

[1] O. F. Hughes and J. K. Paik, Ship Structural Analysis and Design. Alexandria, VA: SNAME, 2010.

[2] R. D. Blevins, Formulas for Natural Frequency and Mode Shape. Malabar, FL: Krieger, 2001.

[3] J. R. Davis, Ed., Aluminum and Aluminum Alloys. Materials Park, OH: ASM International, 1993.

[4] A. Aradhye and D. Joglekar, "Adiabatic guided wave propagation through a honeycomb composite sandwich structure with smoothly varying core thickness," Int. J. Solids Struct., vol. 214-215, pp. 92-109, 2021.

[5] L. Capineri and A. Bulletti, "Ultrasonic guided-wave sensors and integrated SHM systems for impact detection: A review," Sensors, vol. 21, no. 9, p. 2929, 2021.

[6] Q. Shen, O. Schmicker, L. Buhring, and N. Netsch, "Ultrasonic guided wave damage detection for stiffened plates based on deep learning," Ultrasonics, vol. 117, p. 106524, 2021.

[7] O. F. Hosseinabadi and M. R. Khedmati, "A review on ultimate strength of aluminium structural elements for marine applications," Ocean Eng., vol. 232, p. 109153, 2021.

[8] D. K. Kim, S. H. Kim, and M. S. Kim, "Ultimate strength formula for stiffened panels under axial compression using ANSYS-based database," Thin-Walled Struct., vol. 131, pp. 1-15, 2018.

[9] D. K. Singh and S. K. Duggal, "Analysis of stiffened plates using FEM: A parametric study," Int. J. Eng. Res. Technol., vol. 4, no. 5, pp. 635-638, 2015.

[10] M. D. Goel, V. A. Matsagar, and A. K. Gupta, "Blast resistance of stiffened sandwich panels with closed-cell aluminium foam," Lat. Am. J. Solids Struct., vol. 11, no. 13, pp. 2497-2515, 2014.

[11] K. N. Anyfantis, "Ultimate strength of stiffened panels subjected to non-uniform thrust," Int. J. Nav. Archit. Ocean Eng., vol. 12, pp. 325-342, 2020.

[12] J. P. T. P. de Queiroz, M. L. Cunha, A. Pavlovic, and L. A. O. Rocha, "Geometric optimization of stiffened corrugated panels under uniform transverse load," Appl. Mech., vol. 1, no. 3, pp. 153-172, 2020.